RESEARCH ARTICLE | SEPTEMBER 30 2022

Active impedance matching of a cryogenic radio frequency resonator for ion traps
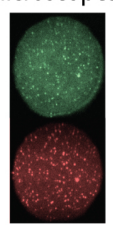
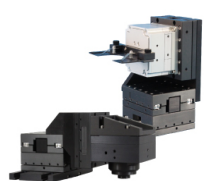M. Schubert ✉ 🔘 ; L. Kilzer; T. Dubielzig; M. Schilling 🔘 ; C. Ospelkaus 🔘 ; B. Hampel 🔘

Check for updates

View Online

Export Citation

AIP Publishing

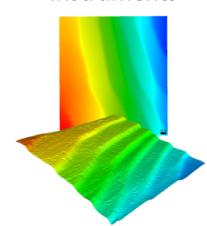# Active impedance matching of a cryogenic radio frequency resonator for ion traps

View Online   Export Citation   CrossMark

M. Schubert,[1,a] 🆔 L. Kilzer,[2] T. Dubielzig,[2] M. Schilling,[1] 🆔 C. Ospelkaus,[2,3] 🆔 and B. Hampel[1] 🆔

AFFILIATIONS

[1] Institut für Elektrische Messtechnik und Grundlagen der Elektrotechnik, TU Braunschweig, Hans-Sommer Strasse 66, 38106 Braunschweig, Germany
[2] Institut für Quantenoptik, Leibniz Universität Hannover, Welfengarten 1, 30167 Hannover, Germany
[3] Physikalisch-Technische Bundesanstalt, Bundesallee 100, 38116 Braunschweig, Germany

[a] Author to whom correspondence should be addressed: marjan.schubert@tu-bs.de

ABSTRACT

A combination of direct current (DC) fields and high amplitude radio frequency (RF) fields is necessary to trap ions in a Paul trap. Such high electric RF fields are usually reached with the help of a resonator in close proximity to the ion trap. Ion trap based quantum computers profit from good vacuum conditions and low heating rates that cryogenic environments provide. However, an impedance matching network between the resonator and its RF source is necessary, as an unmatched resonator would require higher input power due to power reflection. The reflected power would not contribute to the RF trapping potential, and the losses in the cable induce additional heat into the system. The electrical properties of the matching network components change during cooling, and a cryogenic setup usually prohibits physical access to integrated components while the experiment is running. This circumstance leads to either several cooling cycles to improve the matching at cryogenic temperatures or the operation of poorly matched resonators. In this work, we demonstrate an RF resonator that is actively matched to the wave impedance of coaxial cables and the signal source. The active part of the matching circuit consists of a varactor diode array. Its capacitance depends on the DC voltage applied from outside the cryostat. We present measurements of the power reflection, the Q-factor, and higher harmonic signals resulting from the nonlinearity of the varactor diodes. The RF resonator is tested in a cryostat at room temperature and cryogenic temperatures, down to 4.3 K. A superior impedance matching for different ion traps can be achieved with this type of resonator.

I. INTRODUCTION

Atomic ions trapped in a radio frequency (RF) Paul trap are a well-controlled quantum system that has been used in quantum logic applications such as quantum computing,[1,2] quantum simulation,[3] and frequency metrology.[4] While important milestones for quantum logic operations such as ground state cooling of the quantized motional degrees of freedom have been reached in room temperature (RT) setups,[5,6] systems with many ions and especially surface electrode traps[7,8] profit immensely from cooling below 30 K[9] and the resulting lower vacuum pressure and lower ion heating rates.

A Paul trap uses a combination of RF and direct current (DC) fields to generate a trapping potential. For surface-electrode traps, the required voltage is usually of the order of 100 V. Because of Joule

heating and RF crosstalk, this high voltage should not be applied to the long RF cables that run from room temperature to the cold stage of the cryostat.[10] Instead, a step-up resonator close to the trap is used.

The context of the present work is the development of microwave near-field based quantum operations[11,12] carried out on $^9Be^+$ ions in surface-electrode ion traps[13–15] in a cryogenic environment.[16] Most ion trap setups use helical resonators,[17–19] whose key properties are given by their geometry. Cooling them down to cryogenic temperatures not only lets them shrink, but also changes their electrical characteristics, mainly their resistance. This leads to changes in the RF incoupling and quality factor that are sometimes hard to predict, thereby making them unfriendly to use. Lumped-element resonators do not suffer from geometry changes as much as helical resonators do and have been used in some experiments.[10]

05 July 2024 08:15:25

However, both types of resonators lack the ability to *in situ* tune the incoupling to achieve the best possible impedance matching between the source and the trap.

The dimensioning of a matching circuit was described by Gandolfi *et al.*[10] and Brandl *et al.*[20] In particular, for scenarios where traps will be designed, fabricated, and tested in an iterative process, their impedance may differ in each case. The necessary adjustments of system components therefore need to be minimized. Remodeling the resonator when switching between similar trap designs should be avoided for a fast commissioning. Therefore, a matching network that can be controlled electrically from the outside of the vacuum chamber to match a wider band of impedances would be a desirable solution. Varactor diodes have already been used for compensation of phase shifts in a different trap design, where several RF voltages are necessary.[21,22] In this paper, we use varactor diodes for a voltage-controlled impedance matching network.

II. CIRCUIT DESIGN

The development of the resonator and the matching network is based on the circuit model depicted in Fig. 1. It shows the source of the RF signal, which operates at room temperature outside the cryostat. Using coaxial cables, the signal is passed to the resonator box with the matching network and a coil located on a printed circuit board (PCB) next to the ion trap.

The coil L and the capacitance of the ion trap C_{trap} form a series resonant circuit. The coil is made from a silver wire with a diameter of 1.2 mm wound on a bobbin made of polyetheretherketone (PEEK). The bobbin is threaded to prevent the wire from slipping. The coil has a length of 18 mm, a diameter of 9.8 mm, and 6 windings. The ion trap has a capacitance of $C_{\text{trap}} \approx 10$ pF.

The impedance $\underline{Z}_{\text{resonator}}$ for a series resonator is the sum of the coil impedance $j\omega L_{\text{coil}}$, the impedance of the trap capacitance $(j\omega C_{\text{trap}})^{-1}$, and the resistance of the resonator, which is dominated by the wire of the coil R_{coil},

$$\underline{Z}_{\text{resonator}} = R_{\text{coil}} + j\omega L + \frac{1}{j\omega C_{\text{trap}}}. \tag{1}$$

Supplying the circuit with the resonance frequency reduces $\underline{Z}_{\text{resonator}}$ to R_{coil} with

$$\underline{Z}_{\text{resonator}} = R_{\text{Coil}} \ll Z_0 = 50 \ \Omega. \tag{2}$$

A simplified method of matching a resonator to the source impedance with an L-network by using only one reactance is explained in Gandolfi *et al.*[10] in detail. A parallel resonant circuit requires the matching reactance—either a capacitor or an inductor—to be placed in series with the resonant circuit. As part of the matching reactance, the varactor diodes would be exposed to high voltages. In contrast, the matching reactance of a series resonant circuit must be designed in parallel with the resonant circuit, which decreases the voltage at the diodes significantly. Therefore, a series resonant circuit was chosen for the resonator designed in this work.

The resulting matching circuit consists of a parallel capacitance C_{offset} and an active matching network. Both are depicted in Fig. 2. C_{offset} consists of a fixed ceramic capacitor and a ceramic chip trimmer capacitor (Knowles JZ400HV 8–40 pF) for fast adjustments. The active matching network consists of varactor diodes (MACOM MA46H204), whose voltage dependent capacitance can be used to control the overall capacitance of the matching network.

The capacitance of the varactor diodes $D_{1...8}$ can be controlled by applying the voltage V_{bias} from outside the cryostat. The dynamic range of the capacitance of the complete matching network is $(3.7–23.4 \ \text{pF}) + C_{\text{offset}}$ at room temperature. The capacitors C_1 and C_2 decouple the control DC voltage (V_{bias}) from the RF signal, while $L_{1,2,3}$ prevent a short circuit of the RF signal via connections to the DC voltage source.

The "back to back" connection of the varactors divides the adjustable range of the network in halves, but ensures that the characteristic curve of the varactor capacitance, which is approximately proportional to $(V_{\text{bias}})^{-1}$, is slightly linearized around the operating point. This is important, as the voltage of the RF signal also changes the capacitance periodically. Despite the linearization, the matching network is expected to generate mixing products in the form of higher harmonics of the excitation frequency.

The matching network and the resonator coil are located on a PCB in a shielding box made of copper sheet with a thickness of 0.5 mm. This reduces the coupling between the RF signal and other electronic components. The connection between the coil and the ion trap is made with an unshielded cable. Any shielding would add a parasitic capacitance that affects the resonance frequency and the matching.[16]
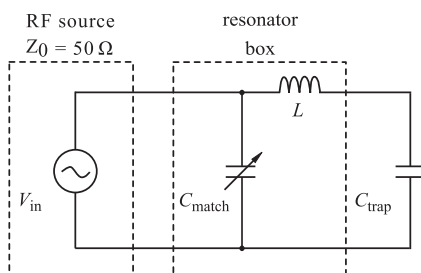
FIG. 1. Schematic of electronic components, including the signal generator as the RF source, the resonator box consisting of the matching network and a coil, and the trap capacitance.
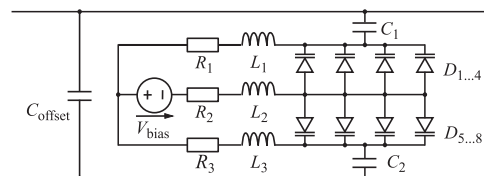
FIG. 2. Circuit of the matching network containing the varactors, the bias voltage V_{bias}, the offset capacitance C_{offset}, and the capacitors and inductors that separate the AC circuit from the DC circuit.

05 July 2024 08:15:25

III. CRYOGENIC APPARATUS AND TEST SETUP

An RDK-415E two-stage Gifford–McMahon cryocooler in conjunction with a F50H compressor by Sumitomo Cryogenics Group (SHI) was used to cool down the RF resonator and the ion trap to cryogenic temperatures. The full test setup is shown in Fig. 3.

An isolation vacuum is established around the two cooling stages of the cryocooler to prevent icing and to reduce the thermal load. A radiation shield inside the vacuum chamber shields the second cooling stage from black body radiation of the vacuum chamber, which is at room temperature (RT). The radiation shield is connected to the first cooling stage, where a higher thermal load can be tolerated compared to the second stage. The isolation vacuum is established through a vacuum pump (Agilent X3580A). The pressure is measured next to the pump (Agilent FRG-700). Another vacuum gauge is installed at the top of the vacuum chamber to provide a complementary pressure measurement. A Lakeshore Model 335 is used for temperature control via DT-670B-CU sensors at the first and second stage of the cryostat. Temperatures of 4.3 K and pressures in the range 10^{-7} to 10^{-9} mbar were reached for all low temperature data that are presented in this paper.

Inside the vacuum chamber, two cables (GVL Cryoengineering GVLZ175) connect to the varactor diodes via D-Sub pins. The varactor diode voltage V_{bias} is provided by two grounded BNC connector feedthroughs. These are connected on the air-side with two RG-58 cables, which are split into conductor and ground lines and

FIG. 3. Schematic drawing of the cryogenic apparatus and the test setup. Electrical DC cables are depicted as dotted lines and AC cables are depicted as dotted-dashed lines. The temperature sensor cables are shown as dashed lines.

FIG. 4. In (a), a CAD rendering of the test setup is shown. The radiation shield is not displayed for visibility reasons. In (b), a photo of the actual RF resonator box is shown, with one side of the copper shield removed.

then connected to the DC supply via banana plugs. A digital power supply (Rigol DP832) provides the V_{bias}.

RF signals are routed into the vacuum chamber via two floating SMA feedthroughs. For simplicity of the test setup, the coaxial cables inside the vacuum chamber are not thermalized on the first cooling stage, but are connected directly to the devices at the second cooling stage with Allectra 311-KAP50S coaxial cables. Two cables of this type, with lengths of 550 and 620 mm, connect to the RF input socket of the resonator and to an ion trap electrode, which in the aforementioned scenario of quantum logic operations induced by microwave near-fields would be used to carry microwave currents and is therefore connected to the outside via RF-compatible cables. This electrode is further referenced as the microwave meander (MWM).[23] The RF output of the resonator box and the RF input of the ion trap PCB are connected with a 120 mm long, shielding-stripped 311-KAP50S.

On the air-side, a signal generator (Siglent SDG2122X) and a vector network analyzer (VNA) Rohde & Schwarz ZVL3 are connected to the cryostat via RG-58 cables. The calibration of the VNA removes the influence of the air-side cables.

A rendering of the test setup and a picture of the RF resonator box is shown in Fig. 4. The test setup is attached to the second stage of the cryocooler. A copper structure was mounted to the second stage to provide thermalization and attachment points. The ion trap on its corresponding PCB, a temperature sensor, and the resonator box are attached to this copper structure. The ground potential of the RF resonator box is connected to the general ground of the setup via the copper structure. The PCB of the ion trap is connected to the same copper structure and thus to the same ground potential. Both, PCB and ion trap, are duplicates of a running quantum logic experiment.[16]

IV. MEASUREMENTS

The evaluation of the circuit is based on the measurement of the reflection parameter, the calculation of the loaded quality-factor (Q-factor), and the suppression of harmonic frequency components of the excitation frequency, which can be expected from nonlinear varactors. In Fig. 5, the corresponding measurement setups used for the following evaluation are shown.

The quality factor is an indicator for the losses in a resonant circuit. A high Q-factor suggests a higher voltage step-up of the trap voltage by the resonator. To determine the Q-factor from the reflection parameter S_{11}, the data were fit to a function that takes the Ohmic losses and frequency dependent damping of the coaxial cables into account.[16] The Q-factors were calculated for every adjusted voltage V_{bias}.

A. Power reflection and Q-factor

The first setup was designed to measure the power reflection coefficient S_{11} through a connection from the VNA to the RF resonator input. This setup is shown in Fig. 5(a). DC voltages V_{bias} were applied to measure the influence of the varactor diodes on the impedance matching. Figure 6(a) shows room temperature measurements of the S_{11} parameter as a function of frequency and for different values of V_{bias}. The matching could be achieved with a fixed capacitance of 100 pF and adjusting the trimmer capacitance
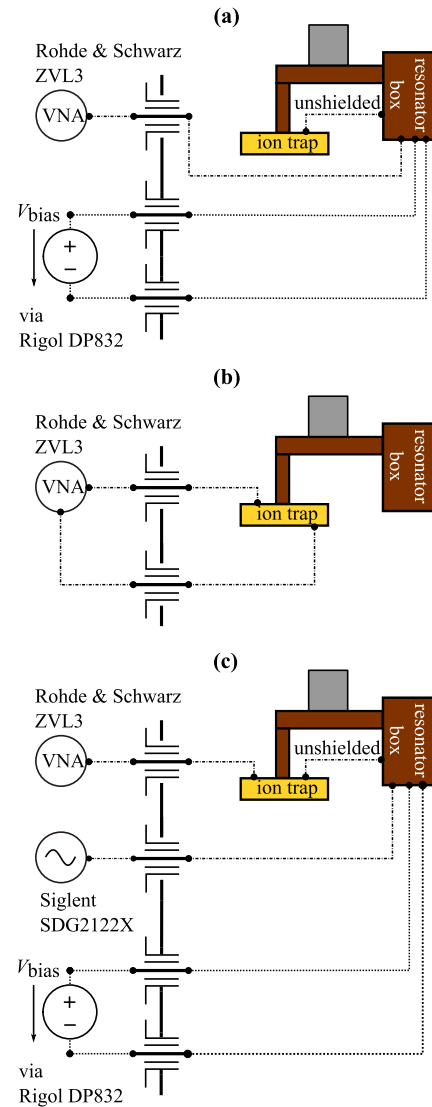

FIG. 5. Schematic drawing of measurement setups. (a) Power reflection of the resonator is measured via the S_{11} parameter. Influence on the impedance matching by the varactor diodes is investigated by applying DC voltages V_{bias}. The input signal is investigated in (b) and (c) for harmonics of the trap voltage. (b) To determine the power transmission loss transfer function from cross-coupling of the RF and MWM lines, $S_{11\text{-RF-MWM}}$ and $S_{21\text{-RF-MWM}}$ are measured. The VNA connects to the MWM and RF lines of the ion trap, without the resonator box in the signal chain. (c) Transmitted power over the ion trap electrodes from cross-coupling of the RF and MWM lines is measured via applying RF voltages of 5 V_{pp} at resonance frequency to the resonator by the signal generator (Siglent SDG2122X). DC voltages V_{bias} were applied to investigate a potential influence of the varactor diodes on the transmitted power.

to 40 pF, resulting in C_{offset} = 140 pF. This capacitance was found by simulating the circuit with LTspice. The Q-factor for the optimal matching with V_{bias} = 2.1 V was calculated to 33.6 for RT data shown in Fig. 6(a).

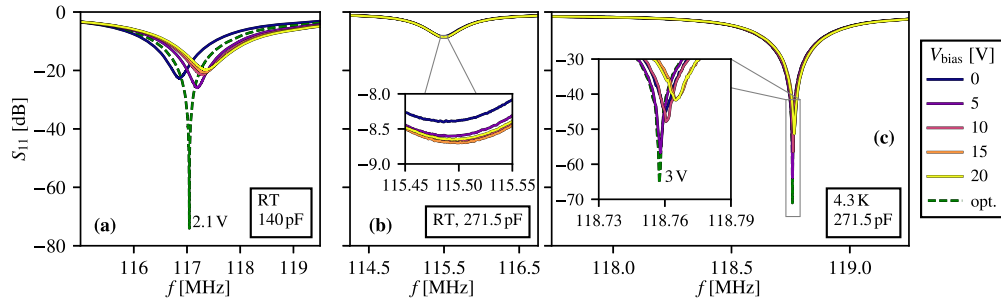05 July 2024 08:15:25

FIG. 6. Power reflection coefficient S_{11} as a function of frequency for five different V_{bias} measured at room temperature (RT) and at 4.3 K. Optimal S_{11} for V_{bias} different from the 5 V increments is displayed in dashed lines. In (a), data of an RT-optimized matching with C_{offset} = 140 pF are shown. In (b), data of a setup with C_{offset} = 271.5 pF at RT are presented, which are optimized for a matching at 4.3 K, as shown in (c).

During cooldowns of the test setup commissioning phase, we observed only small changes in the resonant frequency (≈3%), but significant changes in the incoupling. It could be deduced that the dominant effect for this change in network matching is an increase in conductivity. The matching capacitance has to be set to a value that is too big for a matching at room temperature to compensate the impedance shift caused by the falling temperatures when cooling the experiment to cryogenic temperatures—we call this state overcoupled.

For the cryogenic matching, the fixed capacitance is 240 pF. The trimmer capacitor was set to a value of ~31.5 pF, which results in C_{offset} = 271.5 pF. Figure 6(b) shows S_{11} at RT, and Fig. 6(c) shows the same system at 4.3 K. The optimal matching in Fig. 6(c) was achieved with a bias voltage of V_{bias} = 3 V. For this V_{bias}, the Q-factor was calculated to 212 for the cryogenic data shown in Fig. 6(c).

On comparison of Figs. 6(a) and 6(c), it is noticed that the range between the minimal and maximal reflection parameters is smaller in the cryogenic measurement. The first reason for the smaller range is the decreasing capacitance of the GaAs varactors when cooling to cryogenic temperatures.[24] The second reason is that the value of C_{offset} was increased by a factor of 1.9. In relation to this, the range of the adjustable capacitance becomes smaller as well. Thus, if a larger

setting range is pursued to compensate both effects, the number of varactor diodes should be increased.

Q-factors for all the data shown in Figs. 6(a) and 6(c) are listed in Table I. The values indicate no direct correlation between the quality of the impedance matching and the Q-factor. In addition, the Q-factor increases in the cryogenic experiment, which also indicates lower Ohmic losses.

B. Power transmission

To examine if the amplified trap voltage contains harmonics of the input signal, the spectrum of the voltage must be analyzed. The power was measured indirectly based on cross-coupling to the adjacent MWM electrode of the ion trap to avoid influence due to electrical properties with a measurement setup. These electrodes are used as the pickup device for RF signals produced by the RF electrodes nearby.

First, the coupling between the RF electrodes and the MWM was determined. For this, the resonator box was disconnected from the trap, and the RF and MWM connections of the trap were connected to the VNA. This setup is shown in Fig. 5(b). After cooling down, the reflection and transmission parameters of the system $S_{11-RF-MWM}$ and $S_{21-RF-MWM}$ were measured. The $S_{21-RF-MWM}$ parameter represents the transfer function under the assumption of a two-port network from the RF input to the MWM. We calculated the frequency dependent loss transfer function $H(f)$ from RF to MWM, based on Eqs. (3) and (4), which show the definitions of the $S_{11-RF-MWM}$ and $S_{21-RF-MWM}$ parameters,

$$S_{11-RF-MWM} = 10 \cdot \log_{10}\left(\frac{P_{reflected}}{P_{input}}\right), \quad (3)$$

$$S_{21-RF-MWM} = 10 \cdot \log_{10}\left(\frac{P_{transmitted}}{P_{input}}\right). \quad (4)$$

The ratio of the transmitted power $P_{transmitted}$ and the non-reflected power were required for the transfer function $H(f)$,

$$H(f) = 10 \cdot \log_{10}\left(\frac{P_{transmitted}}{P_{input} - P_{reflected}}\right). \quad (5)$$

TABLE I. Table of measured minimum S_{11} data and the corresponding Q-factors for different V_{bias}. Data are shown for the setups measured at RT, with C_{offset} = 140 pF on the center left side, and at 4.3 K, with C_{offset} = 271.5 pF on the right side of the table. Data points denoted "X" were not measured for the corresponding setup.

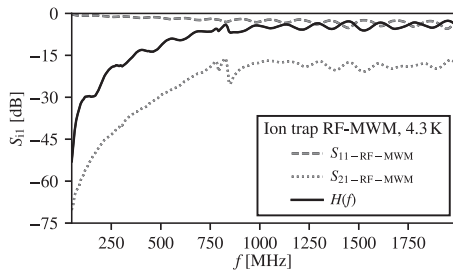| V_{bias} (V)	RT, C_{offset} = 140 pF		4.3 K, C_{offset} = 271.5 pF	
	S_{11} (dB)	Q-factor	S_{11} (dB)	Q-factor
0	−22.7	35.5	−44.9	213.9
2.1	−74.0	33.6	X	X
3	X	X	−65.4	212.0
5	−21.5	31.4	−56.8	212.0
10	−20.7	30.4	−47.9	211.9
15	−25.9	29.9	−41.4	212.9
20	−19.8	29.7	−41.7	211.1

FIG. 7. Reflection parameter $S_{11\text{-RF-MWM}}$, transmission parameter $S_{21\text{-RF-MWM}}$, and loss transfer function $H(f)$ from cross-coupling measurement of the RF and MWM lines on the ion trap without a connected resonator box.

Inserting Eq. (3) into Eq. (5) led to

$$H(f) = S_{21-\text{RF}-\text{MWM}} \cdot \frac{1}{1 - S_{11-\text{RF}-\text{MWM}}}. \qquad (6)$$

The measured S-parameters $S_{11\text{-RF-MWM}}$ and $S_{21\text{-RF-MWM}}$ and the calculated loss transfer function $H(f)$ are shown in Fig. 7.

The resonator box was reconnected to the ion trap after the determination of $H(f)$, and the system was cooled again. RF voltages of 5 V_{pp} at resonance frequency were applied to the RF resonator by the signal generator. This setup is shown in Fig. 5(c). The reassembly shifted the resonance frequency of the system to $f_0 = 116.27$ MHz. The signal at the microwave port was analyzed for multiples n of the excitation frequency using the spectrum analyzer available in the VNA. To check the dependency of the spectrum on the bias voltage, the measurement was repeated for $V_{\text{bias}} = 0, 10,$ and 20 V. The resulting values for different voltages V_{bias} were then corrected with the parameter $H(f)$ and are shown in Fig. 8.

The ion trap used in this setup was designed for $^9\text{Be}^+$.[14] At 22.3 mT, $^9\text{Be}^+$ exhibits a first-order magnetic field-independent qubit transition. We have calculated the frequency range of the ground state hyperfine transitions, which can be used for quantum logic operations, to be between 854 and 1764 MHz. This corresponds to a range of the seventh to the 16th harmonic of the fundamental of the RF signal. Accidental excitation of those transitions would disturb the logic operations. Figure 8 shows that the power levels drop
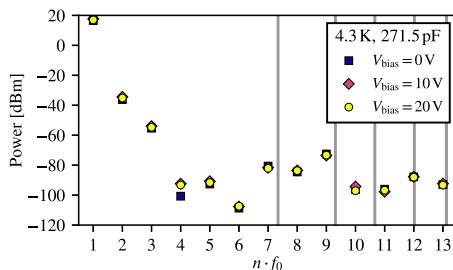

FIG. 8. Harmonics n of the resonance frequency f_0 caused by the nonlinearity of the varactor diodes, depending on the voltage V_{bias}. First-order magnetic field-independent qubit transitions of $^9\text{Be}^+$ ions at 22.3 mT used in the quantum logic experiment[16] are presented in gray color. These frequencies indicate where unsuppressed harmonics could accidentally drive qubit transitions.

below −70 dBm in the relevant frequency ranges. The power level of the second harmonic is already 60 dB suppressed compared to the fundamental. The power of frequencies $n > 13$ dropped below the noise floor.

Without testing, the influence of the measured signals on the qubit remains unknown. However, as the typical hyperfine qubit transitions are magnetic dipole transitions, any influence on the qubit would be due to AC magnetic fields resulting from AC currents due to the periodic recharging of parasitic capacitance in the trap by the trap drive. Unless a harmonic of the trap drive hits the qubit frequency directly, stronger effects would typically arise from the fundamental if it is too close to one of the Zeeman transitions, which can be of the order of 100 MHz for typical long-lived intermediate-field qubit states.[25] Such effects can be avoided through a reasonable choice of the drive frequency.

V. CONCLUSIONS

We have shown that varactor diodes can be used in room temperature and cryogenic setups to match the impedance of a resonator to reduce the power reflection to nearly zero. The adjustability allows us to operate different traps without applying changes to the matching circuit. If the dynamic range of the capacitance is not sufficient to match a larger quantity of impedances, the range can be increased by adding more varactors. The power in the frequency range relevant for ion manipulation is strongly suppressed such that the use of the active matching network is not expected to influence the ions. The new resonator concept can significantly speed up the execution of test campaigns for ion trap designs.

AUTHOR DECLARATIONS

Conflict of Interest

The authors have no conflicts to disclose.

Author Contributions

M. Schubert: Conceptualization (equal); Data curation (equal); Formal analysis (equal); Methodology (equal); Writing – original draft (equal); Writing – review & editing (equal). **L. Kilzer**: Data curation (equal); Formal analysis (equal); Visualization (equal); Writing – original draft (equal); Writing – review & editing (equal). **T. Dubielzig**: Supervision (equal); Writing – original draft (equal); Writing – review & editing (equal). **M. Schilling**: Methodology (equal); Validation (equal); Writing – original draft (equal);

DATA AVAILABILITY

The data that support the findings of this study are available from the corresponding author upon reasonable request.

REFERENCES

[1] T. Monz, D. Nigg, E. A. Martinez, M. F. Brandl, P. Schindler, R. Rines, S. X. Wang, I. L. Chuang, and R. Blatt, "Realization of a scalable Shor algorithm," Science **351**, 1068–1070 (2016).

[2] S. Debnath, N. M. Linke, C. Figgatt, K. A. Landsman, K. Wright, and C. Monroe, "Demonstration of a small programmable quantum computer with atomic qubits," Nature **536**, 63–66 (2016).

[3] T. Schaetz, C. R. Monroe, and T. Esslinger, "Focus on quantum simulation," New J. Phys. **15**, 085009 (2013).

[4] A. D. Ludlow, M. M. Boyd, J. Ye, E. Peik, and P. O. Schmidt, "Optical atomic clocks," Rev. Mod. Phys. **87**, 637–701 (2015).

[5] F. Diedrich, J. C. Bergquist, W. M. Itano, and D. J. Wineland, "Laser cooling to the zero-point energy of motion," Phys. Rev. Lett. **62**, 403 (1989).

[6] C. Monroe, D. M. Meekhof, B. E. King, S. R. Jefferts, W. M. Itano, D. J. Wineland, and P. Gould, "Resolved-sideband Raman cooling of a bound atom to the 3D zero-point energy," Phys. Rev. Lett. **75**, 4011–4014 (1995).

[7] J. Chiaverini, R. B. Blakestad, J. Britton, J. D. Jost, C. Langer, D. Leibfried, R. Ozeri, and D. J. Wineland, "Surface-electrode architecture for ion-trap quantum information processing," Quantum Inf. Comput. **5**, 419–439 (2005).

[8] S. Seidelin, J. Chiaverini, R. Reichle, J. J. Bollinger, D. Leibfried, J. Britton, J. H. Wesenberg, R. B. Blakestad, R. J. Epstein, D. B. Hume, W. M. Itano, J. D. Jost, C. Langer, R. Ozeri, N. Shiga, and D. J. Wineland, "Microfabricated surface-electrode ion trap for scalable quantum information processing," Phys. Rev. Lett. **96**, 253003 (2006).

[9] J. Chiaverini and J. M. Sage, "Insensitivity of the rate of ion motional heating to trap-electrode material over a large temperature range," Phys. Rev. A **89**, 012318 (2014).

[10] D. Gandolfi, M. Niedermayr, M. Kumph, M. Brownnutt, and R. Blatt, "Compact radio-frequency resonator for cryogenic ion traps," Rev. Sci. Instrum. **83**, 084705 (2012).

[11] C. Ospelkaus, C. E. Langer, J. M. Amini, K. R. Brown, D. Leibfried, and D. J. Wineland, "Trapped-ion quantum logic gates based on oscillating magnetic fields," Phys. Rev. Lett. **101**, 090502 (2008).

[12] C. Ospelkaus, U. Warring, Y. Colombe, K. R. Brown, J. M. Amini, D. Leibfried, and D. J. Wineland, "Microwave quantum logic gates for trapped ions," Nature **476**, 181 (2011).

[13] M. Wahnschaffe, H. Hahn, G. Zarantonello, T. Dubielzig, S. Grondkowski, A. Bautista-Salvador, M. Kohnen, and C. Ospelkaus, "Single-ion microwave near-field quantum sensor," Appl. Phys. Lett. **110**, 034103 (2017).

[14] H. Hahn, G. Zarantonello, M. Schulte, A. Bautista-Salvador, K. Hammerer, and C. Ospelkaus, "Integrated ^{9}Be$^+$ multi-qubit gate device for the ion-trap quantum computer," npj Quantum Inf. **5**, 70 (2019).

[15] G. Zarantonello, H. Hahn, J. Morgner, M. Schulte, A. Bautista-Salvador, R. F. Werner, K. Hammerer, and C. Ospelkaus, "Robust and resource-efficient microwave near-field entangling ^{9}Be$^+$ gate," Phys. Rev. Lett. **123**, 260503 (2019).

[16] T. Dubielzig, S. Halama, H. Hahn, G. Zarantonello, M. Niemann, A. Bautista-Salvador, and C. Ospelkaus, "Ultra-low-vibration closed-cycle cryogenic surface-electrode ion trap apparatus," Rev. Sci. Instrum. **92**, 043201 (2021).

[17] W. Macalpine and R. Schildknecht, "Coaxial resonators with helical inner conductor," Proc. IRE **47**, 2099–2105 (1959).

[18] J. R. Fisk, Helical-resonator design techniques, QST, 1976.

[19] J. D. Siverns, L. R. Simkins, S. Weidt, and W. K. Hensinger, "On the application of radio frequency voltages to ion traps via helical resonators," Appl. Phys. B **107**, 921–934 (2012).

[20] M. F. Brandl, P. Schindler, T. Monz, and R. Blatt, "Cryogenic resonator design for trapped ion experiments in Paul traps," Appl. Phys. B **122**, 157 (2016).

[21] M. Kumph, M. Brownnutt, and R. Blatt, "Two-dimensional arrays of radio-frequency ion traps with addressable interactions," New J. Phys. **13**, 073043 (2011).

[22] M. Kumph, P. Holz, K. Langer, M. Meraner, M. Niedermayr, M. Brownnutt, and R. Blatt, "Operation of a planar-electrode ion-trap array with adjustable RF electrodes," New J. Phys. **18**, 023047 (2016).

[23] T. Dubielzig, "Ultra-low vibration closed-cycle cryogenic surface-electrode ion trap apparatus," Ph.D. thesis, Leibniz Universität Hannover, 2021.

[24] M. Nikl, P. Fabeni, G. P. Pazzi, A. Ranfagni, D. Mugnai, B. Sopko, G. Ventura, and K. Sassoli, "GaAs based varicap as tunable capacitance at millikelvin temperatures," Cryogenics **34**, 773–775 (1994).

[25] C. Langer, R. Ozeri, J. D. Jost, J. Chiaverini, B. DeMarco, A. Ben-Kish, R. B. Blakestad, J. Britton, D. B. Hume, W. M. Itano, D. Leibfried, R. Reichle, T. Rosenband, T. Schaetz, P. O. Schmidt, and D. J. Wineland, "Long-lived qubit memory using atomic ions," Phys. Rev. Lett. **95**, 060502 (2005).

05 July 2024 08:15:25